# Sieving of Hot Gases by Hyper-Cross-Linked Nanoscale-Hybrid Membranes

Michiel J. T. Raaijmakers,[†] Mark A. Hempenius,[‡] Peter M. Schön,[‡] G. Julius Vancso,[‡] Arian Nijmeijer,[†] Matthias Wessling,[§] and Nieck E. Benes*,[†]

[†]Inorganic Membranes and [‡]Materials Science and Technology of Polymers, University of Twente, Faculty of Science and Technology, MESA+ Institute for Nanotechnology, P.O. Box 217, 7500 AE Enschede, The Netherlands
[§]Chemical Process Engineering-AVT.CVT, RWTH Aachen University, Turmstrasse 46, 52056 Aachen, Germany

S *Supporting Information*
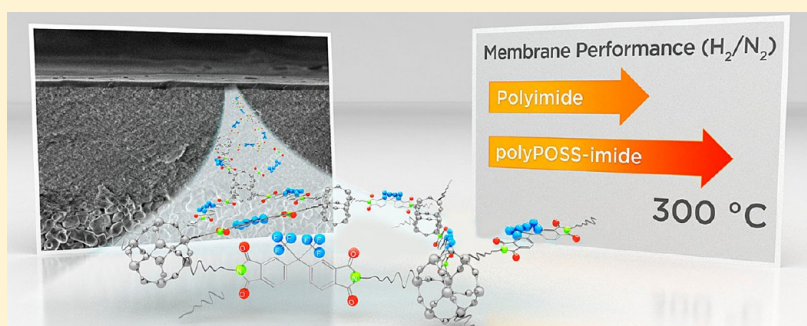
ABSTRACT: Macromolecular networks consisting of homogeneously distributed covalently bonded inorganic and organic precursors are anticipated to show remarkable characteristics, distinct from those of the individual constituents. A novel hyper-cross-linked ultrathin membrane is presented, consisting of a giant molecular network of alternating polyhedral oligomeric silsesquioxanes and aromatic imide bridges. The hybrid characteristics of the membrane are manifested in excellent gas separation performance at elevated temperatures, providing a new and key enabling technology for many important industrial scale applications.
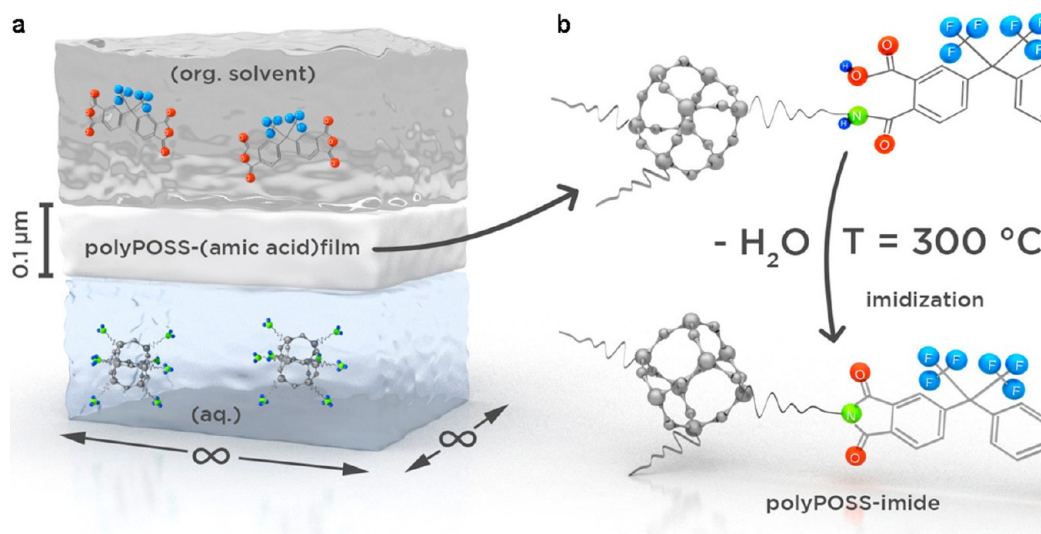
INTRODUCTION

Membrane separation of hot gases is a key enabling technique for many large-scale chemical processes and advanced energy production technologies.[1] Today, no membranes exist that allow selective separation of hot small gas molecules on a large scale. At elevated temperatures, state-of-the-art organic polymer membranes exhibit increased macromolecular dynamics,[2] whereas a high polymer chain rigidity is a prerequisite for effective molecular sieving.[3] The separation performance of even very rigid polymers, such as polyimides, subsides above 200 °C.[2b,4] Novel high temperature polymers such as polybenzimidazoles, and thermally rearranged poly-(benzoxazole)s and poly(benzoxazole-co-imides) have the potential to overcome the temperature limitations of polymers, but until now, relatively few data are available for high temperature applications.[5] In addition, recent advances in nanoengineering of materials have resulted in radically different synthesis approaches for nanostructured membranes and thin films.[6] These systems may well approach the ultimate gas separation performance, yet tremendous efforts are required to allow defect-free processing at the scale of industrially relevant applications. Here, we present a method for the facile production of ultrathin films of inorganic−organic hybrid materials that provide gas separation selectivity up to 300 °C, in combination with chemical versatility and large-scale defect-free processability. The unprecedented characteristics of these membranes originate from the hyper-cross-linked periodic network of covalently bound organic and POSS moieties.

The polyPOSS−imide material presented consists of polyhedral oligomeric silsesquioxane (POSS) molecules, covalently linked by aromatic imide bridges. Cross-linked aromatic polyimides are considered high potential membrane materials.[7] The POSS are silicon oxide cages with the basic formula $R_nSi_nO_{1.5n}$ ($n = 6, 8, 12$) and are decorated with various organo-functional groups. Their cubic symmetry and the availability of a large variety of functional groups allows for nanoscale assembly in three dimensions.[8] The rigidness and bulky character of POSS cages is manifested by the free volume increase observed in systems were POSS is dispersed in the polymer matrix or covalently attached to the polymer main chain.[9] However, such systems are still governed by the macromolecular dynamics of the polymer main chain. Instead, we propose to use the POSS cage as a main building block for the polymer network. We suggest the synthesis of a hybrid polyPOSS−imide film using a two-step procedure: the

Scheme 1. The Membrane Synthesis Process[a]

[a](a) Interfacial polymerization reaction of octa-ammonium POSS in water and 6-FDA in toluene. The ammonium groups are partially deprotonated to primary amines by sodium hydroxide (NaOH, pH = 9.9 ± 0.3). The reaction occurs at the water−toluene interface, with final layer polyPOSS−(amic acid) thicknesses of ∼0.1 μm after 5 min. (b) The subsequent conversion of the amic acid to cyclic imide (imidization) is performed via heat treatment at temperatures up to 300 °C.
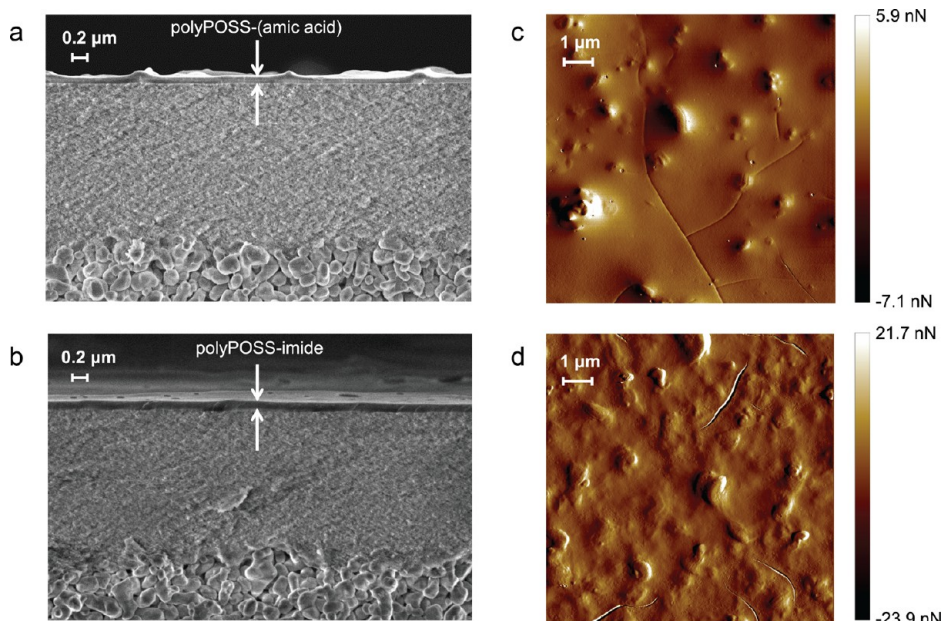

Figure 1. Heat treatment induced evolution of membrane layer morphology. (a and b) SEM micrograph of 0.1-μm polyPOSS−(amic acid) and polyPOSS−imide layers, on α-alumina discs with a 3 μm-thick γ-alumina layer. The homogeneous supported films exhibit no apparent crack formation due to drying stresses or heat treatment. (c and d) The AFM peak force error images of the supported polyPOSS−(amic acid) demonstrate that the film formation results in a smooth layer with hills and valleys of lateral dimensions up to 0.2 μm. The polyPOSS−imide (bottom, right) layer exhibits a similar hill-valley structure. The heat-treatment step increases the intrinsic and thermal stress-induced surface roughness.

interfacial polycondensation of an ammonium chloride salt-functionalized POSS and hexafluoroisopropylidene dianhydride (6-FDA) based on a concept proposed by Dalwani et al.,[10] followed by thermal imidization. In the first step, a thin-film polyPOSS−(amic acid) network is formed via a polycondensation reaction at the interface between two immiscible solvents (Scheme 1a). A water-soluble octa-ammonium POSS in alkaline solution and 6-FDA in toluene were used as the amine and anhydride sources, respectively. In the second step,

the amic acid groups are converted into cyclic imide groups via thermal imidization at temperatures up to 300 °C in either air or an inert atmosphere (Scheme 1b).

■ EXPERIMENTAL SECTION

Synthesis of PolyPOSS−Imides by Interfacial Polymerization. Toluene (anhydrous 99.8 wt %, Sigma-Aldrich), 4,4-(hexafluoroisopropylidene) diphthalic anhydride (6-FDA, Sigma-Aldrich), ammonium chloride salt functionalized POSS (OctaAmmonium POSS, Hybrid Plastics (USA)) and sodium hydroxide (1.0 mol
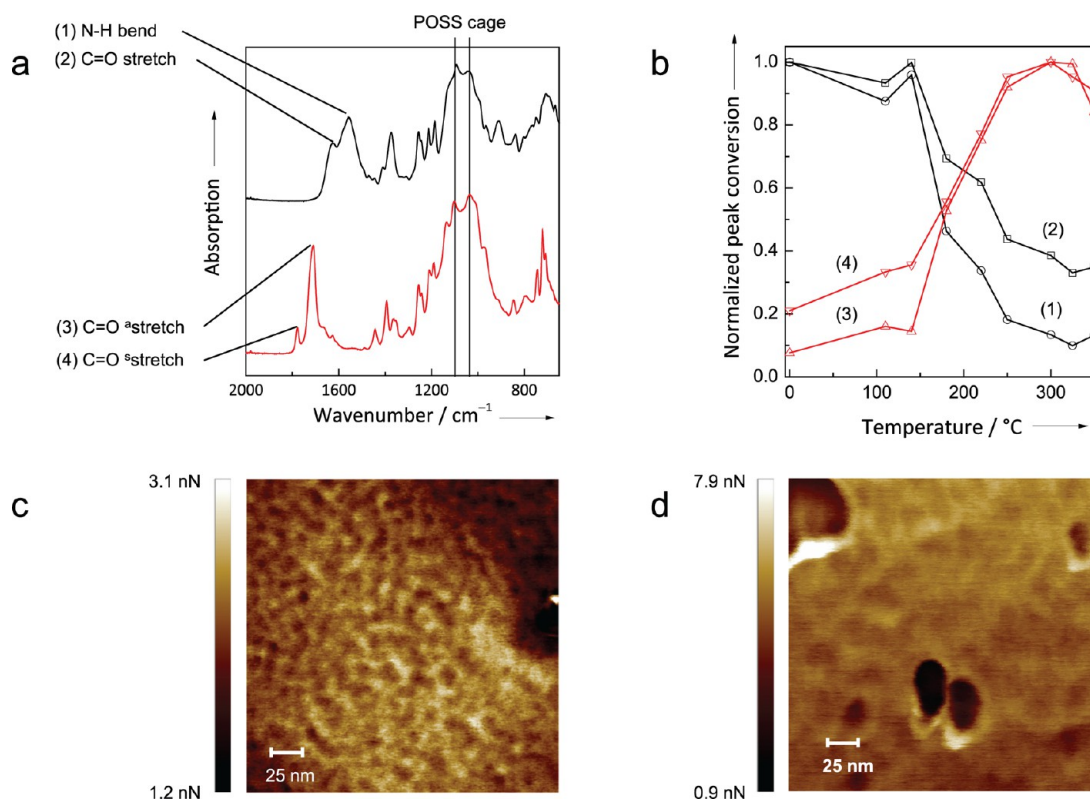
331

dx.doi.org/10.1021/ja410047u | J. Am. Chem. Soc. 2014, 136, 330−335

Figure 2. Heat treatment induced imidization. (a) ATR-FTIR spectra of free-standing polyPOSS−(amic acid) layers prior to (top line) and after heat treatment for 2 h in air at 300 °C (bottom line), normalized for the CF_3 band at 1254 cm^{-1}. The bands at 1620 and 1570 cm^{-1} are assigned to N−H bending (1) and C=O stretching (2) of the amic acid group. After heat treatment, the bands at 1620 and 1570 cm^{-1} are replaced by bands at 1720 and 1780 cm^{-1} that are assigned to C=O asymmetric (3) and symmetric (4) stretching of the imide group, respectively. The sharp bands at 1125 and 1040 cm^{-1} can be attributed to the Si−O−Si asymmetric stretching vibrations of the polyhedral and ladder silsesquioxane structures, respectively. The results indicate complete conversion of the amic acid groups to cyclic imide groups, and suggest a concurrent partial cleavage of the POSS cage induced by the high pH during synthesis.[12] (b)ATR-FTIR band intensities of (1) and (2) normalized with respect to their initial intensities and the band intensities of (3) and (4) normalized with respect to the imide band intensity of the 300 °C-treated sample as a function of temperature. The results indicate that imidization is initiated at 140−160 °C, reaching a maximum conversion at 300 °C. (c and d) AFM adhesion images of polyPOSS−(amic acid) and polyPOSS−imide layers. The images reveal homogeneously distributed areas of several nanometers in size with varying adhesion strength that correspond to regions with different chemical compositions.

L^{-1}) were used as received. Free-standing hybrid films were prepared by adjusting the pH of an aqueous solution of 0.9 wt % ammonium chloride salt functionalized POSS (OctaAmmonium POSS, Hybrid Plastics (USA)), by adjusting the pH to 9.9 using sodium hydroxide (0.1 mol L^{-1}), and subsequently contacting the aqueous solution with a 6-FDA solution in toluene (0.075 wt %). The reaction at the interface between the aqueous POSS solution and 6-FDA in toluene was confirmed by observing the thin-film formation. The mechanical integrity of the films was sufficient for their removal from the interface. The rapid kinetics of the polycondensation reaction allow for the production of a sufficient amount of freestanding film for bulk material characterization, such as infrared spectroscopy. Detailed thin-film characterization was performed on the supported thin films that were produced directly on ceramic membranes (α-alumina discs with a 3-μm-thick γ-alumina layer). Film formation atop porous alumina supports was achieved by soaking the porous ceramic material in the aqueous POSS solution, followed by contacting with the 6-FDA solution in toluene. The membrane was thermally imidized at 300 °C at a heating rate of 5 °C/min^{-1} under an air atmosphere.

Material Characterization. Static liquid/air contact angles were measured with a goniometer (OCA 15, Data Physics). Drops of 1 μL Milli-Q water were formed at the needle tip and contact angles were measured 5 s after placing the drop on the substrate. Density measurements were performed using an AccuPyc II 1340 gas displacement density analyzer (Micromeritics), with helium as gas source. The polyPOSS−(amic acid) and polyPOSS−imide samples were placed in a vacuum chamber, at 30 °C, prior to the measurement

to remove any water from the sample. The standard deviation was determined from 30 separate density measurements. Scanning electron microscopy (SEM) images were obtained using a LEO-1550 Schottky field emission scanning electron microscope (Carl-Zeiss, Germany), with an accelerating voltage of 2.00 kV.

Atomic Force Microscopy (AFM) measurements were performed using a Multimode 8 AFM instrument equipped with a NanoScope V controller, and a vertical engage J-scanner (Bruker AXS, Santa Barbara, CA). Membrane samples were glued to a metal support using a two component epoxy and dried overnight. Image processing and data analysis were performed with NanoScope software version 8.14 and NanoScope Analysis software version 1.40. Peak force tapping was done in air with Si tips on SiN cantilevers (SCANASYST-AIR, Bruker AXS, Camarillo, CA; nominal spring constant 0.4 N/m). Cantilever spring constants were determined with the thermal noise method. Imaging was done with a peak force tapping amplitude of 150 nm and at a scan rate of 0.97 Hz.

Membrane single gas permeation experiments were performed in a dead-end mode at a trans-membrane pressure of 2 bar, and atmospheric pressure at the permeate side. Once the helium permeance remained constant, the other gases (N$_2$, CH$_4$, H$_2$, and CO$_2$, consecutively) were measured at temperatures between 50 and 300 °C.
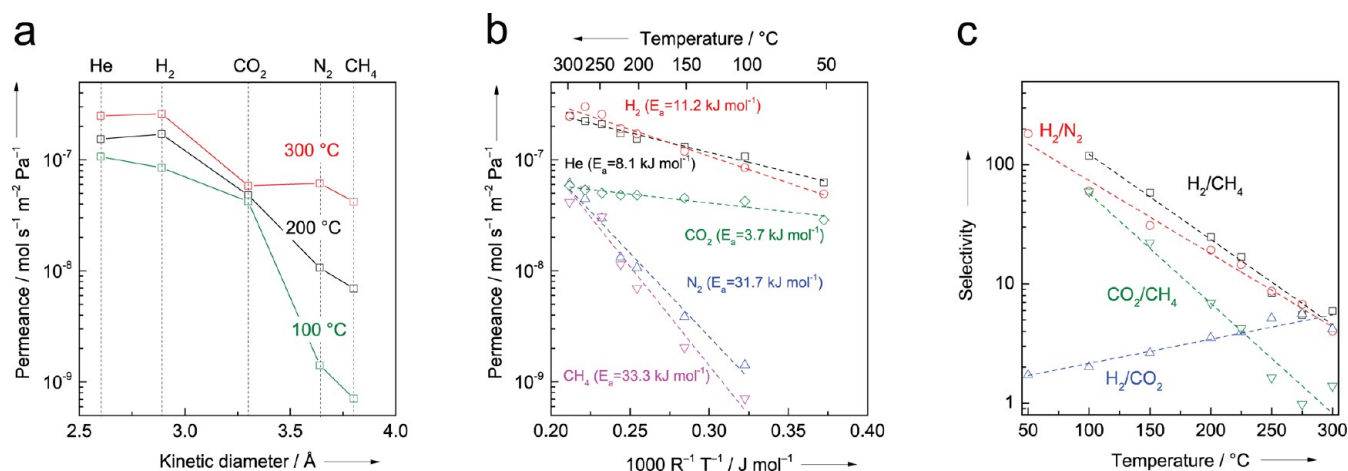
Figure 3. Gas permeation characteristics of polyPOSS–imide membranes. (a) Permeance as a function of gas kinetic diameter. The decrease in permeance with increasing kinetic diameter is consistent with the glassy character of the polyPOSS–imide. (b) Arrhenius plot of individual gas permeances for He, H_2, CO_2, N_2 and CH_4. For all gases, activated transport is the dominant transport mechanism. The activation energies for transport remain constant over temperatures ranging from 50–300 °C, demonstrating that the membrane does not suffer from temperature-induced chain mobility. (c) Ideal selectivity of H_2/CH_4, H_2/N_2, CO_2/CH_4 and H_2/CO_2 as a function of temperature.

RESULTS AND DISCUSSION

Film formation was confirmed using scanning electron microscopy (SEM) cross section images, and top-view atomic force microscopy (AFM) as depicted in Figure 1. The SEM micrograph reveals a distinct continuous film of approximately 0.1 μm atop the ceramic support. The AFM top-view topography image of the polyPOSS–(amic acid) reveals a smooth top layer with height differences (0.1 μm) and a morphology less coarse compared to that of typical layers obtained via interfacial polymerization.[11] Figure 1b,d corresponds to the polyPOSS–imide layer obtained after thermal imidization at 300 °C. The SEM micrograph demonstrates that a distinct and continuous film remains on the support. The AFM images do exhibit a change in morphology resulting from stresses in the thin film confined on the porous support. Density measurements via pycnometry on the freestanding film material reveal that these stresses originate from densification, with the bulk density increasing from 1.47 to 1.63 g/cm³, induced by the chemical conversion of the amic acid groups to cyclic imides. However, no cracks appear to form in the ultrathin films. The high degree of cross-linking and the limited thickness of this layer prevent any pinhole or crack formation that could degrade the membrane's gas separation performance.

The formation of the polyPOSS–(amic acid) and its subsequent conversion to polyPOSS–imide via thermal treatment are confirmed using Fourier transform infrared spectroscopy with attenuated total reflectance (FTIR-ATR). Figure 2a presents the spectra of the samples before and after thermal imidization at 300 °C. The untreated sample exhibits two typical polyamide bands at 1620 and 1570 cm^{-1} that correspond to C=O stretching and N–H bending, respectively. After thermal treatment, these two bands vanish, and two distinct bands emerge at 1720 and 1780 cm^{-1} that can be attributed to polyimide C=O symmetric and asymmetric stretching, respectively. The thermal conversion to polyimide is not inhibited by the presence of water, whereas trace water removal is a main challenge in the synthesis of polyimides via polymerization in aprotic polar solvents.[13] Figure 2b displays the intensities of the two amic acid bands at 1570 (1) and 1620 cm^{-1} (2) and of the imide bands at 1720 (3) and 1780 cm^{-1}

(4). The spectra are normalized with respect to the C–F band intensity at 1254 cm^{-1}. At temperatures below 140 °C, no imidization occurs. The onset of imidization is observed between 140 and 160 °C, and increases up to 300 °C, above which a decrease in band intensity is observed that can be explained by deimidization and polymer-bond degradation. This result is confirmed via thermogravimetric analysis (TGA) that indicates that there is no weight loss at temperatures up to 300 °C in either air or nitrogen atmospheres (Supporting Information). Figure 2c,d presents the adhesion-force images of polyPOSS–(amic acid) and polyPOSS–imide. Peak force tapping AFM was used to map the adhesion forces of the polyPOSS–(amic acid) and polyPOSS–imide surfaces. The adhesion force was determined from the force–distance curves corresponding to an oscillating AFM tip that contacts the sample upon each oscillation at a rate well below the resonance frequency of the AFM cantilever.[14] The images reveal 1–5-nm sized heterogeneities, bearing resemblance to two-dimensional periodic covalent organic frameworks,[15] that can be attributed to the intrinsic molecular local ordering of inorganic and organic moieties. This local intrinsic ordering remains after the amic acid is converted into the imide; however, the force contrast diminishes. This result can be rationalized through the replacement of the strong polar amic acid with a weakly interacting imide. A comparison of the water contact angle measurements (Supporting Information) of the polyPOSS–(amic acid) (53°) with those of the polyPOSS–imide (72°) suggest a similar effect, supporting a nanoscale evolution in the adhesion force.

The hybrid characteristics of the material are manifested in the exceptional gas separation performance at elevated temperatures. Unprecedented performance at temperatures up to 300 °C (the practical limit of the measurement apparatus) is observed from individual gas permeation experiments. Figure 3 illustrates the gas permeation behavior of polyPOSS–imide on α-alumina discs with a 3-μm-thick γ-alumina layer. Figure 3a depicts a plot of the single gas permeance as a function of the gas molecule kinetic diameter (for He, H_2, CO_2, N_2 and CH_4) at 100, 200, and 300 °C. The permeance decreases with increasing gas molecule kinetic diameter, a trend typical of glassy polymers. Figure 3b depicts the Arrhenius plot of the

permeance on a logarithmic scale as a function of $R^{-1}T^{-1}$, revealing that the gas permeance is thermally activated. The activation energies for the measured gases are in the order CH_4 > N_2 > H_2 > He > CO_2. The polyPOSS−imide activation energies for gas permeation are a factor 5−7 higher as compared to conventional polyimides.[16] The relatively high activation energies for permeation underline the high energy barriers for gas diffusion in the rigid polyPOSS−imide network. The low activation energy for the CO_2 transport results from the high solubility of CO_2 at low temperatures due to the presence of trifluoromethyl groups. At elevated temperatures, this solubility decreases, while the diffusivity increases, canceling out the effect of temperature on the product of these processes. This is in agreement with gas sorption and diffusion data measured for other 6-FDA polyimide membranes.[16,17] These studies show that, for increasing temperature, the CO_2 permeation remains constant or even decreases. The correspondingly low activation energy emanates from the conjunct increase in diffusivity and decrease in sorption, at increasing temperature. For the other gases, He, N_2 and CH_4, the permeation does increase with temperature. The result is a decrease in selectivity of CO_2 over these other gases. Conventional polyimides without trifluoromethyl groups do not display such behavior.[18] The affinity toward CO_2 implies that gas molecules diffuse in the organic part of the network, which is in agreement with the findings of molecular dynamics simulations.[19]

Unlike polymer membranes that suffer from chain-rearrangement-induced permeability loss at the elevated temperatures used in this study, this linear trend in the Arrhenius plot suggests that the activation energies of diffusion and sorption do not significantly depend on the temperature. The high thermal stability of the membrane can be rationalized by the large number of covalent bonds between the individual POSS cages. An average POSS/imide ratio of 3.8 was observed using X-ray photoelectron spectroscopy (XPS) of a polyPOSS−imide on an alumina support (Supporting Information). Figure 3c presents the ideal selectivities of the H_2/CH_4, H_2/N_2, CO_2/CH_4 and H_2/CO_2 gas pairs as a function of the temperature. The persistence of selectivity at elevated temperatures underlines the moderation of augmented macromolecular dynamics in the hyper-cross-linked polyPOSS−imide network. The dilation of the network is impeded by the high large number of organic bridges linking the rigid POSS cages, while molecular motions of the organic bridges allow diffusion of gas molecules.[20] The selectivity as a function of temperature decreases due to the differences in the activation energies between gases, which results in an increase in the H_2/CO_2 selectivity with temperature and a decrease in the selectivities for the other gas pairs. Most surprisingly, the polyPOSS−imide membrane retains gas selectivities of approximately 5 for H_2/CH_4 and H_2/N_2 at 300 °C, which are unsurpassed by any other polymeric membrane. Moreover, the CO_2/CH_4 selectivities of approximately 60 at temperatures below 100 °C emphasize the applicability of the polyPOSS−imide over a broad temperature range.

CONCLUSION

In summary, we have described the preparation of polyPOSS−imide ultrathin gas separation membranes using interfacial polymerization followed by thermal imidization. The interfacial reaction results in an intrinsic homogeneous distribution of inorganic and organic constituents on the molecular scale. The subsequent heat treatment successfully converts the as-formed amic acid into a cyclic imide at temperatures exceeding 180 °C. The hybrid character of the thin film is manifested in its excellent gas separation performance at elevated temperatures, which originate from the hyper-cross-linked periodic network of covalently bound rigid POSS and mobile organic moieties. The presented method can be easily extended to other dianhydride linkers to yield the next generation of potential gas separation membranes for elevated-temperature applications.

ASSOCIATED CONTENT

⑤ Supporting Information

The full reaction scheme of the polyPOSS−imide; material analysis using differential scanning calorimetry, thermal gravimetric analysis, X-ray photoelectron spectroscopy and full infrared peak analysis. This material is available free of charge via the Internet at http://pubs.acs.org.

AUTHOR INFORMATION

Corresponding Author
n.e.benes@utwente.nl

Notes
The authors declare no competing financial interest.

ACKNOWLEDGMENTS

REFERENCES

(1) (a) Niwa, S. I.; Eswaramoorthy, M.; Nair, J.; Raj, A.; Itoh, N.; Shoji, H.; Namba, T.; Mizukami, F. *Science* **2002**, *295*, 105−107. (b) Jiang, H.; Cao, Z.; Schirrmeister, S.; Schiestel, T.; Caro, J. *Angew. Chem., Int. Ed.* **2010**, *49*, 5656−5660. (c) Choudhary, V. R.; Gaikwad, A. G.; Sansare, S. D. *Angew. Chem., Int. Ed.* **2001**, *40*, 1776−1779.

(2) (a) Wind, J. D.; Sirard, S. M.; Paul, D. R.; Green, P. F.; Johnston, K. P.; Koros, W. J. *Macromolecules* **2003**, *36*, 6433−6441. (b) Koros, W. J.; Woods, D. G. *J. Membr. Sci.* **2001**, *181*, 157−166.

(3) (a) Guiver, M. D.; Lee, Y. M. *Science* **2013**, *339*, 284−285. (b) Carta, M.; Malpass-Evans, R.; Croad, M.; Rogan, Y.; Jansen, J. C.; Bernardo, P.; Bazzarelli, F.; McKeown, N. B. *Science* **2013**, *339*, 303−307. (c) Du, N.; Park, H. B.; Robertson, G. P.; Dal-Cin, M. M.; Visser, T.; Scoles, L.; Guiver, M. D. *Nat. Mater.* **2011**, *10*, 372−375. (d) Song, Q.; Cao, S.; Zavala-Rivera, P.; Lu, L. P.; Li, W.; Ji, Y.; Al-Muhtaseb, S. A.; Cheetham, A. K.; Sivaniah, E. *Nat. Commun.* **2013**, *4*, No. 1918.

(4) Rezac, M. E.; Koros, W. J.; Miller, S. J. *J. Membr. Sci.* **1994**, *93*, 193−201.

(5) (a) Calle, M.; Doherty, C. M.; Hill, A. J.; Lee, Y. M. *Macromolecules* **2013**, *46*, 8179−8189. (b) Calle, M.; Lozano, A. E.; Lee, Y. M. *Eur. Polym. J.* **2012**, *48*, 1313−1322. (c) Joseph, W. D.; Abed, J. C.; Mercier, R.; McGrath, J. E. *Polymer* **1994**, *35*, 5046−5050. (d) Kim, S.; Han, S. H.; Lee, Y. M. *J. Membr. Sci.* **2012**, *403−404*, 169−178.

(6) (a) Angelova, P.; Vieker, H.; Weber, N. E.; Matei, D.; Reimer, O.; Meier, I.; Kurasch, S.; Biskupek, J.; Lorbach, D.; Wunderlich, K.; Chen, L.; Terfort, A.; Klapper, M.; Müllen, K.; Kaiser, U.; Gölzhäuser, A.; Turchanin, A. *ACS Nano* **2013**, *7*, 6489−6497. (b) Vendamme, R.; Onoue, S. Y.; Nakao, A.; Kunitake, T. *Nat. Mater.* **2006**, *5*, 494−501. (c) Peinemann, K. V.; Abetz, V.; Simon, P. F. W. *Nat. Mater.* **2007**, *6*, 992−996. (d) Du, N.; Park, H. B.; Dal-Cin, M. M.; Guiver, M. D. *Energy Environ. Sci.* **2012**, *5*, 7306−7322. (e) Ho, B. P.; Chul, H. J.;

Young, M. L.; Hill, A. J.; Pas, S. J.; Mudie, S. T.; Van Wagner, E.; Freeman, B. D.; Cookson, D. J. *Science* **2007**, *318*, 254−258.

(7) Vanherck, K.; Koeckelberghs, G.; Vankelecom, I. F. J. *Prog. Polym. Sci.* **2013**, *38*, 874−896.

(8) (a) Laine, R. M.; Roll, M. F. *Macromolecules* **2011**, *44*, 1073−1109. (b) Nischang, I.; Brüggemann, O.; Teasdale, I. *Angew. Chem., Int. Ed.* **2011**, *50*, 4593−4596. (c) Oaten, M.; Choudhury, N. R. *Macromolecules* **2005**, *38*, 6392−6401. (d) Wu, G.; Su, Z. *Chem. Mater.* **2006**, *18*, 3726−3732. (e) Zhang, C.; Babonneau, F.; Bonhomme, C.; Laine, R. M.; Soles, C. L.; Hristov, H. A.; Yee, A. F. *J. Am. Chem. Soc.* **1998**, *120*, 8380−8391.

(9) (a) Iyer, P.; Iyer, G.; Coleman, M. *J. Membr. Sci.* **2010**, *358*, 26−32. (b) Leu, C. M.; Chang, Y. T.; Wei, K. H. *Chem. Mater.* **2003**, *15*, 3721−3727.

(10) Dalwani, M.; Zheng, J.; Hempenius, M.; Raaijmakers, M. J. T.; Doherty, C. M.; Hill, A. J.; Wessling, M.; Benes, N. E. *J. Mater. Chem.* **2012**, *22*, 14835−14838.

(11) Freger, V. *Langmuir* **2003**, *19*, 4791−4797.

(12) J. Feher, F.; D. Wyndham, K.; Soulivong, D.; Nguyen, F. *J. Chem. Soc., Dalton Trans.* **1999**, 1491−1498.

(13) Sroog, C. E. *Prog. Polym. Sci.* **1991**, *16*, 561−694.

(14) Schön, P.; Bagdi, K.; Molnár, K.; Markus, P.; Pukánszky, B.; Julius Vancso, G. *Eur. Polym. J.* **2011**, *47*, 692−698.

(15) Colson, J. W.; Dichtel, W. R. *Nat. Chem.* **2013**, *5*, 453−465.

(16) Duthie, X.; Kentish, S.; Powell, C.; Nagai, K.; Qiao, G.; Stevens, G. *J. Membr. Sci.* **2007**, *294*, 40−49.

(17) (a) Lin, W. H.; Chung, T. S. *J. Membr. Sci.* **2001**, *186*, 183−193. (b) Tanaka, K.; Okano, M.; Toshino, H.; Kita, H.; Okamoto, K.-I. *J. Polym. Sci., Part B: Polym. Phys.* **1992**, *30*, 907−914.

(18) Villaluenga, J. P. G.; Seoane, B.; Hradil, J.; Sysel, P. *J. Membr. Sci.* **2007**, *305*, 160−168.

(19) Neyertz, S.; Gopalan, P.; Brachet, P.; Kristiansen, A.; Männle, F.; Brown, D. *Soft Mater.* **2014**, *12*, 113−123.

(20) Lin, H.; Van Wagner, E.; Freeman, B. D.; Toy, L. G.; Gupta, R. P. *Science* **2006**, *311*, 639−642.

335

dx.doi.org/10.1021/ja410047u | *J. Am. Chem. Soc.* 2014, 136, 330−335